Glauber like model and multiplicity analysis of identified particles in proton proton collisions at LHC energies

M.Sc. Thesis

By
Pavish Subramani

Discipline Of Physics
INDIAN INSTITUTE OF TECHNOLOGY INDORE
June 2019

Glauber like model and multiplicity analysis of identified particles in proton proton collisions at LHC energies

A Thesis

Submitted in partial fulfillment of the requirements for the award of the degree
of
Master of Science
by
Pavish Subramani

Discipline of Physics
INDIAN INSTITUTE OF TECHNOLOGY INDORE
June 2019

INDIAN INSTITUTE OF TECHNOLOGY INDORE
CANDIDATE'S DECLARATION

I hereby certify that the work which is being presented in the thesis entitled **"Glauber like model and multiplicity analysis of identified particles in proton proton collisions at LHC energies"** in the partial fulfilment of the requirements for the award of the degree of MASTER OF SCIENCE and submitted in the **DISCIPLINE OF PHYSICS, Indian Institute of Technology Indore**, is an authentic record of my own work carried out during the time period from JULY 2018 to JUNE 2019 under the supervision of Dr. Raghunath Sahoo, Associate Professor, Indian Institute of Technology Indore. The matter presented in this thesis has not been submitted by me for the award of any other degree of this or any other institute. In case of any plagiarism, as the sole author, I shall stay responsible.

Pavish Subramani

This is to certify that the above statement made by the candidate is correct to the best of my knowledge.

M.Sc. Thesis Supervisor
(Dr. Raghunath Sahoo)

Pavish Subramani has successfully given his M.Sc. Oral Examination held on ....

(M.Sc. Thesis Supervisor)
Date:

(Convener,DPGC)
Date:

(PSPC Member 1.)
Date:

(PSPC Member 2.)
Date:

Dedicated to my family and people of India

Acknowledgement

My research is an accomplishment built on the strong base of guidance, encouragement, motivation and academic as well as moral support from many people. I would love to acknowledge and thank all of them, who have contributed to and helped me complete my project successfully.

Firstly, I would like to express my sincere thanks to my guide Dr. Raghunath Sahoo for the extensive support in this work. His insight and motivation to excel and deep knowledge lead to successfull understanding and completion of this thesis. He imparted me the wisdom of research being a beautiful meditation, losing into which we can build ourselves.

I record my sincere thanks to my PSPC member Prof. Subhendu Rakshit and Dr. Manavendra N Mahato for their inspiration and support towards academics and research. Their guidance has inspired me to give my best at what I do.

I am immensely thankful to my PSPC member Dr. Anand Parkash for his stimulating discussions and encouragement.

I am deeply indebted to Mr. Suman Deb, Mr. Dhanajaya Thakur and Dr. Golam Sarwar for their guidance and immense help to achieve results.

Most of all, I deeply owe to my father Mr. H. Subramani, mother Mrs. B. Saraswathi and brother Mr. Abinesh Subramani for being with me through thick and thin. I extend my thanks to the rest of my family, and friends who were with me throughout the period of my academic career.

I certainly acknowledge the facilities and resources provided to us by the Indian Institute of Technology Indore.

Pavish Subramani
MSc, Final Year
Discipline of Physics
IIT Indore

Abstract

Quark Gluon Plasma (QGP) is a primordial matter found few microseconds after the Big bang. This thesis presents elementary discussions on Quark Gluon Plasma and its possible signatures in proton-proton collisions. The theory behind QGP formation and its presence in high energy collisions experiments along with open problem explaining need for number of binary collisions of partons in proton-proton collisions to formulate initial conditions using Glauber model is presented. We then discuss methodology for reproducing charged particle distribution using Glauber formulation coupled with negative binomial distribution (NBD). The role of Multi Parton Interaction (MPI) in proton proton collisions along with analysis methodology for understanding identified/ strange/ multi-strange particle production mechanism is studied using PYTHIA8 event generator. We discuss the $< p_T >$, $\frac{dN}{dy}$, particle ratios and newly proposed quantity R_{pp} are determined as a function of charged particle multiplicity at mid and forward rapidities.

Contents

List of Figures

Chapter 1

Introduction

The universe is made up of fundamental particles classified as fermions and bosons. Elementary fermions are of two types namely quarks and leptons. There are six different types of quarks: up, down, charm, strange, top and bottom and six leptons: electron (e^-), electron neutrino (ν_{e^-}), muon (μ^-), muon neutrino (ν_{μ^-}), tauon (τ^-), tauon neutrino (ν_{τ^-}). These quarks and leptons can interact through four interactions: Gravitational, Electromagnetic, Weak and Strong. The Electromagnetic theory description is well understood and is unified with weak interaction in $SU(2)_L \bigotimes U(1)_Y$ gauge symmetry, where gauge bosons are photon and $W^\pm$ and Z bosons. This theory is also called Electroweak theory (1). The theory that describes strong interaction between quarks and gluons (called partons) is Quantum Chromodynamics (QCD).

1.1 Quark Gluon Plasma

QCD has two notable properties: asymptotic freedom and confinement. Asymptotic freedom suggests that the coupling strength becomes arbitarly small (g « 1) for smaller length (order of few fermi) scales or equivalently higher energy/ momentum scale. The number of flavors and number of colors decide whether the theory is asymptotically free or not. The beta function which provides energy dependence (μ) with gauge coupling (g) is defined as (2),

$$\beta(g) = \frac{\partial g}{\partial log\mu} = -\frac{g^3}{(4\pi)^2}\left(\frac{11N_c}{3} - \frac{2N_f}{3}\right) \tag{1.1}$$

In QCD $N_c = 3$, hence number of flavors should be greater than 16 ($N_f > 16$) in order $\beta(g)$ to be positive. Since we have only six flavors of quarks the theory is asymptotically free. Confinement prevents free quark to exist in nature. In the confined phase, the energy required to separate two quarks increases with the sep-

aration distance.
When the confinement is broken due to result of high energy then the resultant phase of nuclear matter will contain relatively free quarks and gluons. This phase is called Quark Gluon Plasma (QGP). Higher temperature and higher baryon density are the recipies for formation of QGP. When the QCD vacuum is excited by increase in temperature, hadrons are formed. When temperature of the system is further increased the hadrons starts to overlap each other. After critical temperature (T_c) roughly about 160 - 180 MeV the hadronic system dissolves into system of quarks and gluons. Similar way, when the overlap occurs adiabatically, at higher baryon density the system dissolves into quarks and gluons. This kind of primordial matter can be found in core of neutron stars or at early universe or at high energy collision experiments (like in LHC) (3) (4).

1.2 High energy collisions in LHC

In heavy ion collisions, two lorentz contracted nuclei with radius of order fermi collide each other. The most of incident partons lose some energy, most of these interactions are soft where only small momentum transfer takes place. This can be explained as follows, two nuclei can be considered as two discs of strongly interacting transverse color fields and the charges associated with these fields collide. Hence some of color charge exchange occurs between these disks and longititudinal color fields are produced. These in turn occupy space between colliding disks thus reducing energy in disks themselves and then they gradually decay into $q\bar{q}$ and gluons (17). There is also less probable high transverse momentum particle production due to hard perturbative interactions between incident partons.

As a consequence of lorentz contraction, the system with very high energy formed just as the two disks collide is very far from equilibrium. This system expands and cools as it does. The energy density after saome time say 1 fm/c where the discs are roughly 2 fm apart are still greater than the average energy density of typical hadrons (18). Thus the quarks and gluons produced after the collisions are far from independent. They form a collective medium because they are strongly coupled and flow as a relativistically hydrodynamic fluid with low viscosity to entropy density ratio ($\frac{\eta}{s} \approx \frac{1}{4\pi}$). This matter is Quark Gluon Plasma.

Due to very short lifetime ($\approx 10^{-23}$ sec) QGP cannot be directly observable. What is observable are hadronic and leptonic residues of the transient QGP state. The main signatures of QGP are direct photon production, enhanced production of strange particles, J/ψ suppression. Recently it was found in high mutiplicity proton proton collisions there is enhancement of strangeness production in ALICE experiment (19). This kind of results allows one to speculate that there might be formation of QGP matter in proton proton collisions also.

1.3 Need for number of binary parton collisions in proton proton collision

It is observed that ratio of yield of particles in Pb-Pb collision to that of p-p collision with scaling of number of binary nucleon-nucleon collisions is less than 1 for central collisions (5). This ratio is called as nuclear modification factor (R_{AA}). This is defined as follows,

$$R_{AA} = \frac{(dN_{AA}/dp_T)}{< N_{coll} > (dN_{pp}/dp_T)} \tag{1.2}$$

The fact that suppression observed in R_{AA} of charged hadrons was an indication that presence of strong medium effect on production of particles in the final states (5).

In order to probe possible medium formation in proton proton collisions, comparison of yield in proton proton collisions at high and low multiplicity has to be taken. Accordingly the formula can be rewritten as

$$R_{pp} = \frac{\left(dN_{pp}/dp_T\right)_{high} / < N_{coll} >_{high}}{\left(dN_{pp}/dp_T\right)_{low} / < N_{coll} >_{low}} \tag{1.3}$$

where yield in corresponding yields are normalised with corresponding mean N_{coll}. The main ingredient for the above formula is mean number of binary parton-partonn collisions ($< N_{coll} >$). Traditional Glauber model is used to find the N_{coll} from either 2pF function or hard sphere distribution of nucleon density in case of heavy-ion collisions considering protons as point like particles. In the same spirit an attempt to extend Glauber model for proton proton collisions are taken in this thesis.

Chapter 2

Estimation of number of binary parton collisions for proton proton collisions

In heavy-ion collisions, the formalism for Glauber is straight forward and same is employed in this thesis. Unlike in heavy-ion collisions where the protons are assumed as the point like particle in most of the models. The density profile usually taken is Wood-Saxon density profile, where the density of nucleons in nucleus is distributed in radially symmetric fashion. But application of point like proton model into proton proton collision will not be a valid conclusion at energies in the order of few TeV because, at higher collision energies the Bjorken variable ($x \propto \frac{1}{\sqrt{s}}$) becomes closer to zero, hence wave function of individual quarks and gluons inside proton becomes dominant. So, proton no longer can be considered a point particle but an extended object with constituent partons. In this thesis, we took complex extended proton as the base model (6). Main objective for this chapter is to emphasis the fact that N_{coll} and hence number of participant partons (N_{part}) can be calculated for proton proton collision and the methodology involved in the same.

2.1 Model description

In this thesis, Gaussian-fluctuating configuration model for describing proton is considered. In this model, proton is made up with three effective quarks and gluon flux tubes connecting them and they interact via harmonic potential which is in accordance with Renormalization group procedure for effective particles (RGPEP) (1).

The densities of quarks (ρ_q) and gluons (ρ_g) itself taken as Gaussian type as

$$\rho_q(\mathbf{r}; r_q) = \frac{1}{(2\pi)^{3/2} r_q^3} e^{-\frac{r^2}{2r_q^2}} \tag{2.1}$$

Three effective quarks with gaussian density profile shifted from each other by distance greater than the RMS radius of the quarks (r_q).

$$\rho_g(\mathbf{r}; r_s, r_l) = \frac{1}{(2\pi)^{3/2} r_s^2 r_l} e^{-\frac{x^2+y^2}{2r_s^2} - \frac{z^2}{2r_l^2}} \tag{2.2}$$

The density distribution of quarks is spherically symmetric about the centre of each quarks with parameter r_q while, density of gluons are cylindrically symmetric about the line joining centres of two adjacent quarks.with radius parameterised by r_s hence, the overall combination of these density profiles becomes radially asymmetric. The radius of the gluon flux tubes (r_s) are determined by the radius of the quarks connected to each end and the length of the tubes will be restricted by the RMS radius of the proton itself.

The overall density function of proton under study was taken to be following,

$$\begin{aligned} \rho_{G-f}(\mathbf{r}; \mathbf{r}_1, \mathbf{r}_2, \mathbf{r}_3) = & N_g \frac{1-\kappa}{3} \sum_{k=1}^{3} \rho_q(\mathbf{r} - \mathbf{r}_k; r_q) \\ & + N_g \frac{\kappa}{3} \sum_{k=1}^{3} \rho_g[\mathscr{R}^{-1}[\theta_k, \phi_k](\mathbf{r} - \frac{\mathbf{r}_k}{2}; r_q, \frac{r_k}{2}] \end{aligned} \tag{2.3}$$

where, $\mathscr{R}[\theta,\phi]$ transforms vector (0,0,1) into $(cos\phi sin\theta, sin\phi cos\theta, cos\theta)$ and $\mathbf{r}_k = r_k(cos\phi_k sin\theta_k, sin\phi_k cos\theta_k, cos\theta_k)$ is the position vector of k-th effective quark. The explicit form of $\mathscr{R}[\theta,\phi]$ is given in Appendix A. At high energies contribution of gluons dominate over quarks in particle production. In order to incorporate the different weights for such contributions, parameter κ is used where, κ can take values $0 < \kappa < 1$ and N_G is the overall normalisation constant.

2.2 Calculation of Overlap function

Assuming the direction of incoming protons to be in z-axis so the collision plane is x-y plane, hence any dependency along z-axis is integrated out.

$$T(x, y) = \int \rho(x, y, z) dz \tag{2.4}$$

The density distribution provides probability of finding parton at (x, y, z), per unit volume normalised to unity. While the thickness function provide the probability of finding a parton at target flux per unit transverse area. The overlap function $T_{pp}(b)$ for projectile proton(a) and target proton(b) is defined as

$$T_{pp}(b) = \int\int T_a(x-\frac{b}{2},y)T_b(x+\frac{b}{2},y)dxdy \tag{2.5}$$

where $T_a(x-\frac{b}{2},y)T_b(x+\frac{b}{2},y)dxdy$ provide the joint probability distribution for finding parton in the overlap region dxdy upon integration provides overlap function. Here T_{pp} is sum of 4-components namely quark-quark, quark-gluon, gluon-quark, gluon-gluon (calculations for the same is not provided explicitely).

$$T_{pp}(b) = (T_{pp})_{qq}(b) + (T_{pp})_{gg}(b) + (T_{pp})_{qg}(b) + (T_{pp})_{gq}(b) \tag{2.6}$$

2.3 Results for calculation of N_{coll}

Number of binary collision between partons given by

$$N_{coll}(b) = \sigma_{gg}^{INEL}T_{pp}(b) \tag{2.7}$$

Where, σ_{gg}^{INEL} is inelastic cross section of partons ($\sigma_{gg}^{INEL} = 4.3$ mb for $p+p$ collision at $\sqrt{s} = 7$TeV). Overlap function is geometric description of collision mechanism, σ introduces energy into equations because σ is dependent on collision energy. Number of participant partons at impact parameter 'b' is given as

$$N_{part}(b) \propto N_{coll}^{x}(b) \tag{2.8}$$

where x is a free parameter ($0 < x < 1$).

The positions of constituent quarks in this model are varied in random and allowed to collide with other proton. Length of the gluon tubes are kept fixed. As it connects two quarks the parameter, d = 1.5 fm. The RMS radius of quarks and protons are taken to be 0.25 fm and 1 fm respectively. Since the inelastic cross section of partons (σ^{INEL}) is known and taken to be 0.43 barn. Giving equal contributions from quarks and gluons for cross section parameter κ is kept as 0.5 and $N_G = 10$. The resultant N_{coll} is obtained as function of impact parameter, b. Impact parameter distribution taken to be gaussian with mean close to RMS radius of proton and as well as 3σ exhausts length approximately RMS diameter of proton. This as input for the model gives for N_{coll} and N_{part} as a function of impact parameter (b).

The Figure 2 shows the comparison of number of binary participant collisions and number of participants in p+p collisions and Au-Au collisions. Overall com-

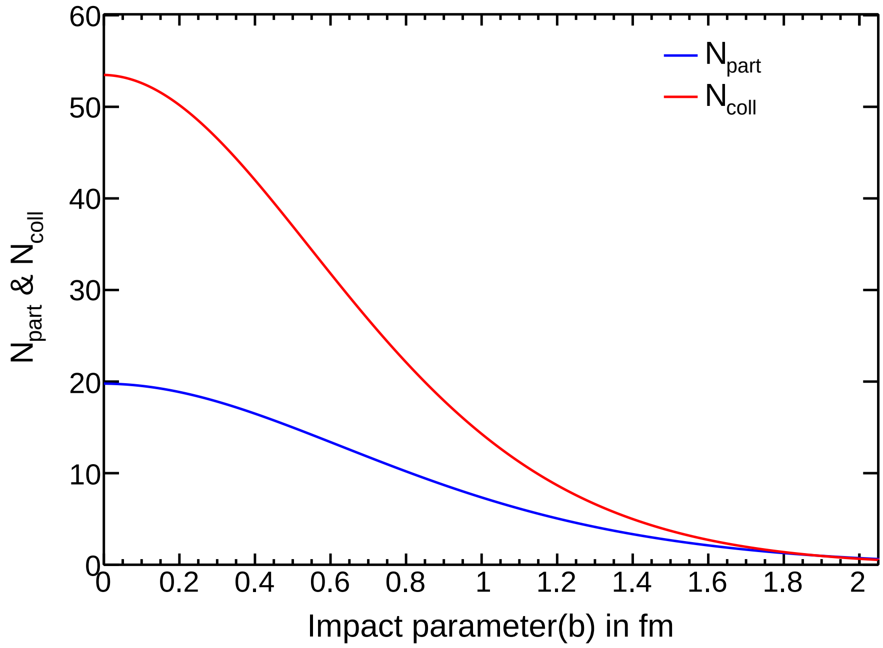

Figure 2.1: (color online) Number of binary parton parton collisions and number of participant partons as function of impact parameter calculated using our model

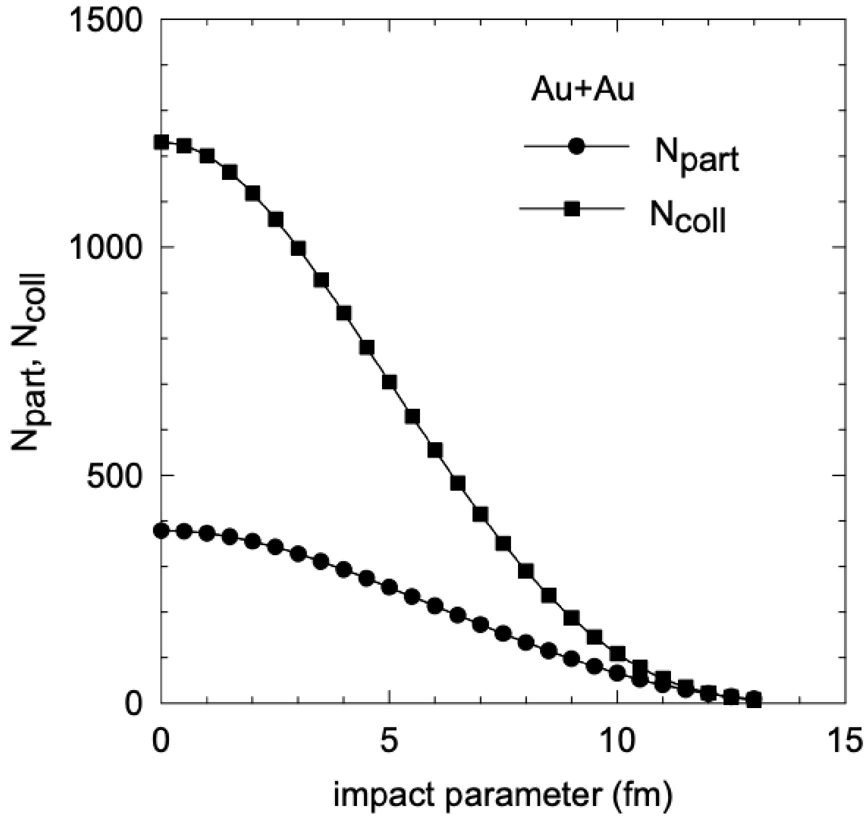

Figure 2.2: (color online) Number of binary nucleon nucleon collisions and number of participant nucleons as function of impact parameter calculated for Au-Au collisions at $\sqrt{s_{NN}} = 200$ GeV

parison reveals for particular choice of parameters the experimental data can be explained well using this model.

Chapter 3

An overview of Multi Parton Interactions in p-p collisions

To understand hadronic collisions at LHC, QCD based partonic models of hadron provide basis. In this base, each hadron is considered to have elementary particles as constituents. These hadron when collide at ultra relativistic velocity the constituents form the seed of the complicated process leading to production of different particles at detector(10). Due to composite nature of hadrons, it is possible to have multiple hard parton scattering in single hadron-hadron collisions. These class of events are known as Multiple Parton Interactions(MPI). Also correlation between N_{MPI} and N_{ch} are not linear in nature. Hence to understand particle production mechanism, the MPI scale is inevitable. Here we used a pQCD inspired monte carlo event generator PYTHIA to analyse particle production mechanism with MPI scale.

3.1 Description of PYTHIA8

PYTHIA is a common tool used to generate events in high energy proton proton collisions. In 1978, JETSET was developed and it was merged with PYTHIA. The older versions of PYTHIA used FORTRON 77 as coding language. PYTHIA8 was designed to have C++ as its coding language. The minimum CM energy that PYTHIA limited is 10 GeV and the maximum can extend upto CM energy of 100 TeV(8).
Hard process included are of $2 \to 1$,$2 \to 2$ and $2 \to 3$ type. QCD processes are classified into hard and soft classes. The soft QCD processes include Elastic processes ($AB \to AB$), Single diffractive ($AB \to XB$ or $AB \to AX$), Double diffractive ($AB \to X$) and Non-Diffractive processes. The Hard QCD includes following processes $gg \to gg$, $gg \to q\bar{q}$, $qg \to qg$, $qq \to qq$, $q\bar{q} \to gg$, $qq \to qq(New)$, $gg \to c\bar{c}$, $q\bar{q} \to c\bar{c}$, $gg \to b\bar{b}$, $q\bar{q} \to b\bar{b}$.

Along with QCD processes PYTHIA includes Electroweak, Higgs processes, Top quark production and also SUSY processes. Hadronisation in PYTHIA is solely on the Lund string fragmentation framework(7). Main ingredient in PYTHIA8 is introduction of Multi parton interactions, which is discussed in next section.

3.2 MPI in PYTHIA8

Perturbative QCD gives as a function of transverse momentum p_T, the total rate of parton-parton interactions(6). In parton based MPI models it is observed that cross sectiion for $2 \to 2$ scattering diverges for low momentum transfers.

$$d\sigma_{2\to 2} \propto \frac{dp_\perp^2}{p_\perp^4} \tag{3.1}$$

Also abandunce of low x partons at high collision energy ($\sqrt{s}$) makes it worse. Thus at LHC energies when this cross section is $p_\perp$ integrated from some $p_{\perp min}$ to some kinetic maximum produces higher cross section than total hadron-hardron cross section for $p_{\perp min}$ of order $(4-5)$ GeV(8). This could be interpreted as that every hadron-hadron collisions contains several parton-parton interactions with typical momentum of order $p_{\perp min}$.
Hence cross section in equation 3.1 can be re-intrepreted such that number of multiparton interactions per collision diverges rather than cross section itself as $p_{\perp min} \to 0$. Ultimately the $p_\perp \to 0$ divergence is tamed by color-screening effects, which provide natural lower cut-off for $p_\perp$. In PYTHIA, the divergence removed by adding cutoff $p_{\perp 0}$ as (11),

$$\frac{d\sigma_{2\to 2}}{dp_\perp^2} \propto \frac{\alpha_S^2(p_\perp^2 + p_{\perp 0}^2)}{(p_\perp^2 + p_{\perp 0}^2)^2} \tag{3.2}$$

The α_S , $p_{\perp 0}$ parameter and parton distribution function (PDF) are tunable aspects of this model. Upon integrating equation 3.2 for inelastic, non-diffractive process we obtain mean number of MPI as,

$$< n_{MPI} > (p_{\perp 0}) = \frac{\sigma_{2\to 2}(p_{\perp 0})}{\sigma_{ND}} \tag{3.3}$$

where σ_{ND} is the non-diffractive cross section for the process.
If all MPI are uncorrelated the above equation holds and the $< n_{MPI} >$ could be considered as the mean of poisson distribution. But in PYTHIA several correlations are considered like energy conservation of partons. This is achieved by ordering MPI into decreasing value of x , where $x = \frac{2p_\perp}{\sqrt{s}}$, so hardest MPI is generated first.

Probability of i-th interaction is given by Sudokov-type expression,

$$\frac{d\mathscr{P}_{MPI}}{p_\perp} = \frac{1}{\sigma_{ND}} \frac{d\sigma_{2\to 2}}{dp_\perp} \exp\left(- \int_{p_\perp}^{p_{\perp i-1}} \frac{1}{\sigma_{ND}} \frac{d\sigma_{2\to 2}}{dp'_\perp} dp' \right) \tag{3.4}$$

where $d\sigma_{2\to 2}$ may now be modified to take correlations with the $(i-1)$ preceding MPI into account.

3.3 Analysis Methodology

Minumum thresold value of p_T to classify the hard QCD is kept at 2 GeV/c to avoid divergence of cross section mentioned in equation 3.1.
To have better control of statistics, we have generated 1.5 Million Events for proton proton collisions at $\sqrt{s}$ = 13 TeV and $\sqrt{s}$ = 7 TeV using PYTHIA8.2. ϕ is reconstructed using Kaon channel ($\phi \to K^- + K^+$) and K^* is reconstructed using Kaon-pion channel ($K^* \to K^+ + \pi^-$). The charged particle muliplicity is measured for both mid - pseudorapidity ($|\eta| < 0.5$) and pseudorapidity range corresponds to V0A and V0C detectors in ALICE, together called V0M detectors ($-3.7 < \eta < -1.7$ and $2.8 < \eta < 5.1$). For R_{pp} analysis six different multiplicity classes in mid - pseudorapidity and V0M pseudorapidity classes as well as N_{MPI} classes were defined as shown in the Table 3.1 similarly for other analysis multiplicity classes is given in the Table 3.2.

Table 3.1: Multiplicity classes

$\|\eta\| < 0.5$	$0 < N_{ch} < 2$ $8 < N_{ch} < 11$	$2 < N_{ch} < 5$ $11 < N_{ch} < 25$	$4 < N_{ch} < 8$
V0M	$0 < N_{ch} < 8$ $25 < N_{ch} < 35$	$8 < N_{ch} < 16$ $35 < N_{ch} < 70$	$16 < N_{ch} < 25$
N_{MPI}	$0 < N_{MPI} < 2$ $8 < N_{MPI} < 11$	$2 < N_{MPI} < 5$ $11 < N_{MPI} < 25$	$4 < N_{MPI} < 8$

Analysis flow chart indicating part of analysis displaying steps for calculation of mean p_T and R_{pp} as a function of charged particle multiplicity is shown in the Figure 3.1.

Table 3.2: Multiplicity classes

$\lvert\eta\rvert < 0.5$	$0 < N_{ch} < 2$	$2 < N_{ch} < 4$	$4 < N_{ch} < 6$
	$6 < N_{ch} < 8$	$8 < N_{ch} < 11$	$11 < N_{ch} < 14$
	$14 < N_{ch} < 18$	$18 < N_{ch} < 22$	$22 < N_{ch} < 27$
V0M	$0 < N_{ch} < 3$	$3 < N_{ch} < 6$	$6 < N_{ch} < 9$
	$9 < N_{ch} < 15$	$15 < N_{ch} < 20$	$20 < N_{ch} < 28$
	$28 < N_{ch} < 38$	$38 < N_{ch} < 50$	$50 < N_{ch} < 70$
N_{MPI}	$0 < N_{MPI} < 2$	$2 < N_{MPI} < 4$	$4 < N_{MPI} < 6$
	$6 < N_{MPI} < 8$	$8 < N_{MPI} < 11$	$11 < N_{MPI} < 14$
	$14 < N_{MPI} < 18$	$18 < N_{MPI} < 22$	$22 < N_{MPI} < 27$

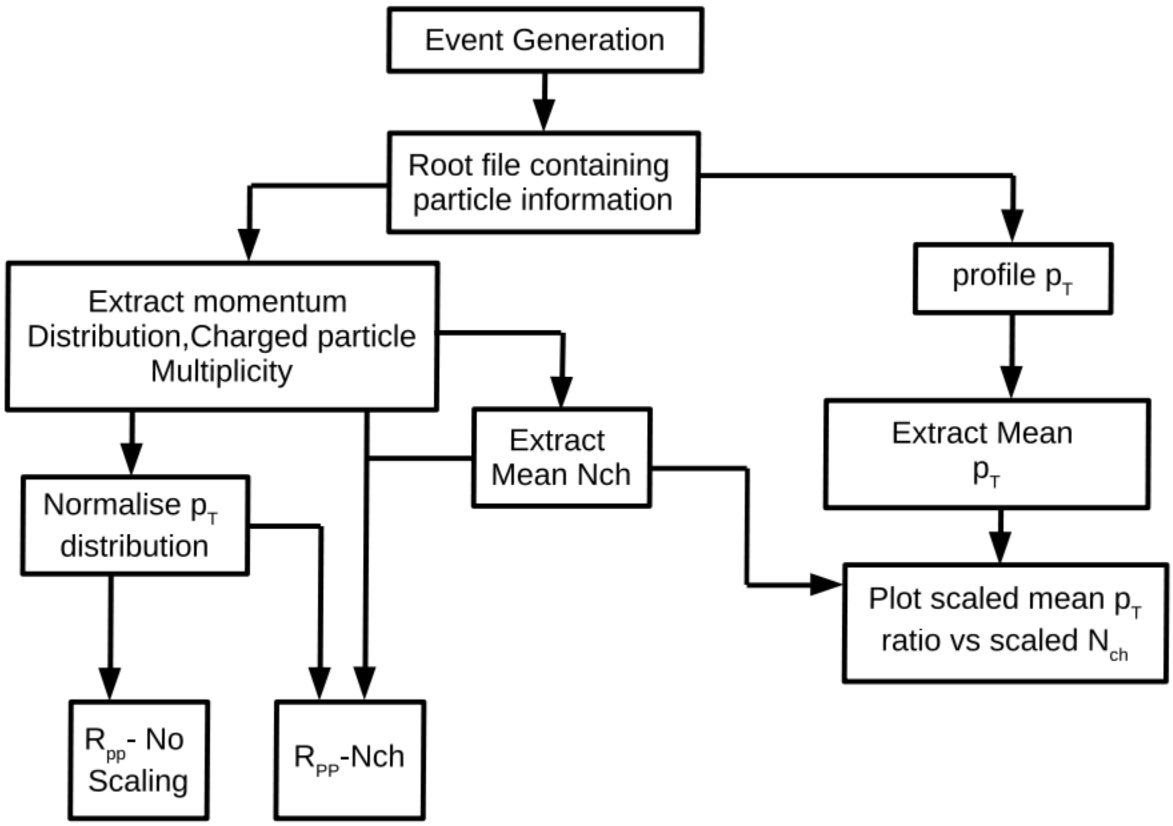

Figure 3.1: Analysis flow chart

Chapter 4

Particle production mechanism in light of MPI scale

Since number of hard scattering is directly proportional to number of charged particles produced in an event, we expect a linear relationship between N_{MPI} and N_{ch}. In fact that is the case when we consider mean characteristics of both as shown in the Figure 4.1, where we observe clear deviation from $y = mx$.

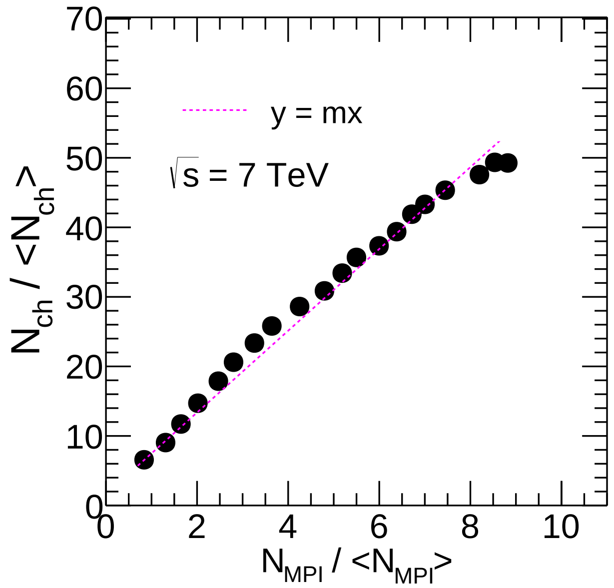

Figure 4.1: (Color online) Correlation plot between N_{ch} and N_{MPI} at $\sqrt{s} = 7 TeV$

However when we project one multiplicity bin of N_{ch} over N_{MPI} we get gaussian like distribution of N_{MPI} with increasing mean corresponding to higher and higher N_{ch} multiplicity shown in plot 4.2.

Hence need for multiplicity study of N_{MPI} is inevitable as like N_{ch}. Different variables and its variation with respect to N_{ch} and N_{MPI} multiplicity bins are discussed in this section.

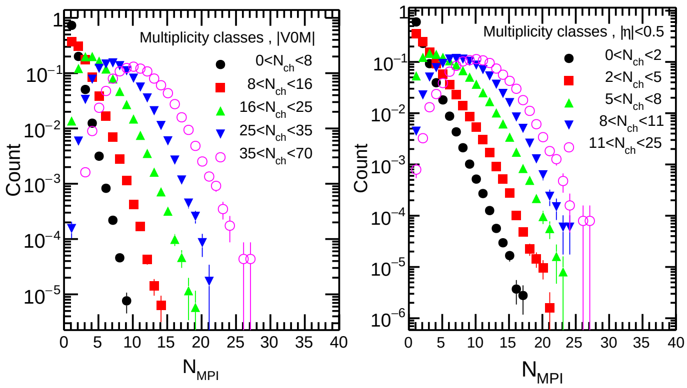

Figure 4.2: (Color online) Projection plots for different N_{ch} classes into N_{MPI}

4.1 R_{pp} analysis

R_{pp} in this analysis is defined as follows,

$$R_{pp-nch} = \frac{\left(dN_{pp}/dp_T\right)_{i-bin} / < N_{ch} >_{i-bin}}{\left(dN_{pp}/dp_T\right)_{min-bias} / < N_{ch} >_{min-bias}} \tag{4.1}$$

$$R_{pp-nmpi} = \frac{\left(dN_{pp}/dp_T\right)_{i-bin} / < N_{MPI} >_{i-bin}}{\left(dN_{pp}/dp_T\right)_{min-bias} / < N_{MPI} >_{min-bias}} \tag{4.2}$$

$$R_{pp-no-scaling} = \frac{\left(dN_{pp}/dp_T\right)_{i-bin}}{\left(dN_{pp}/dp_T\right)_{min-bias}} \tag{4.3}$$

As the replacement for mean number of binary collisions mean N_{ch} for different multiplicity bins are taken since number of hard collisions in an event is directly proportional to N_{ch}.

R_{pp} as a function of p_T for different particles in both high and low multiplicity at 7 and 13 TeV CM energies are plotted (Figures 4.3 4.4 4.5). It is observed that the particle production mechanism for both high and low multiplicity are different due to curves varying slopes relatively negative compared to other. R_{pp} supression ($R_{pp} < 1$) is observed for high multiplicity for $p_T < 1GeV$ and for low multiplicity for $p_T > 1GeV$. And the crossing of curves do not vary for different particles for corresponding different classes of N_{ch} and N_{MPI}.

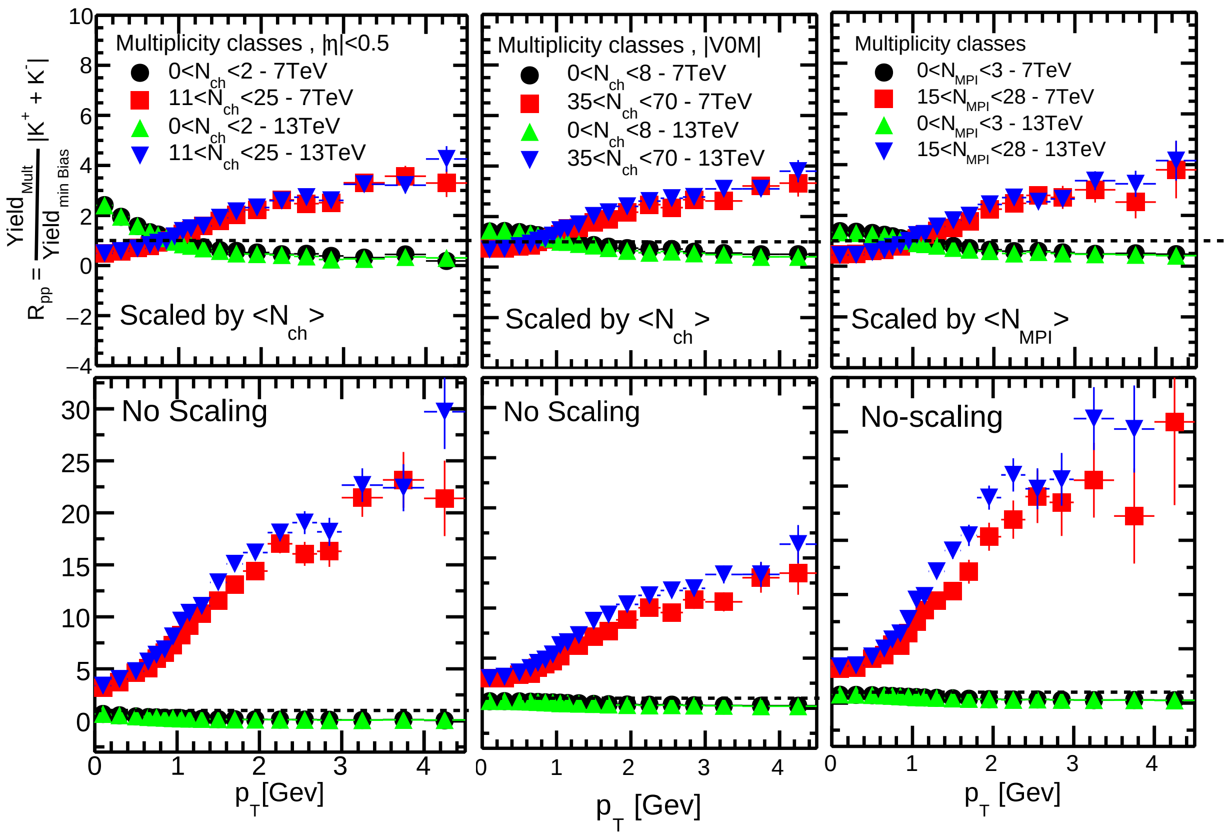

Figure 4.3: (Color online) panel - 1(from left): R_{pp} of kaon as a function of charged particle multiplicity in mid rapidity region. panel - 2: R_{pp} of kaon as a function of charged particle multiplicity in forward rapidity region. panel - 3: R_{pp} of kaon as a function of number of multi-parton interactions for inclusive hard processes using PYTHIA8. The vertical lines in data points are the statistical uncertainties.

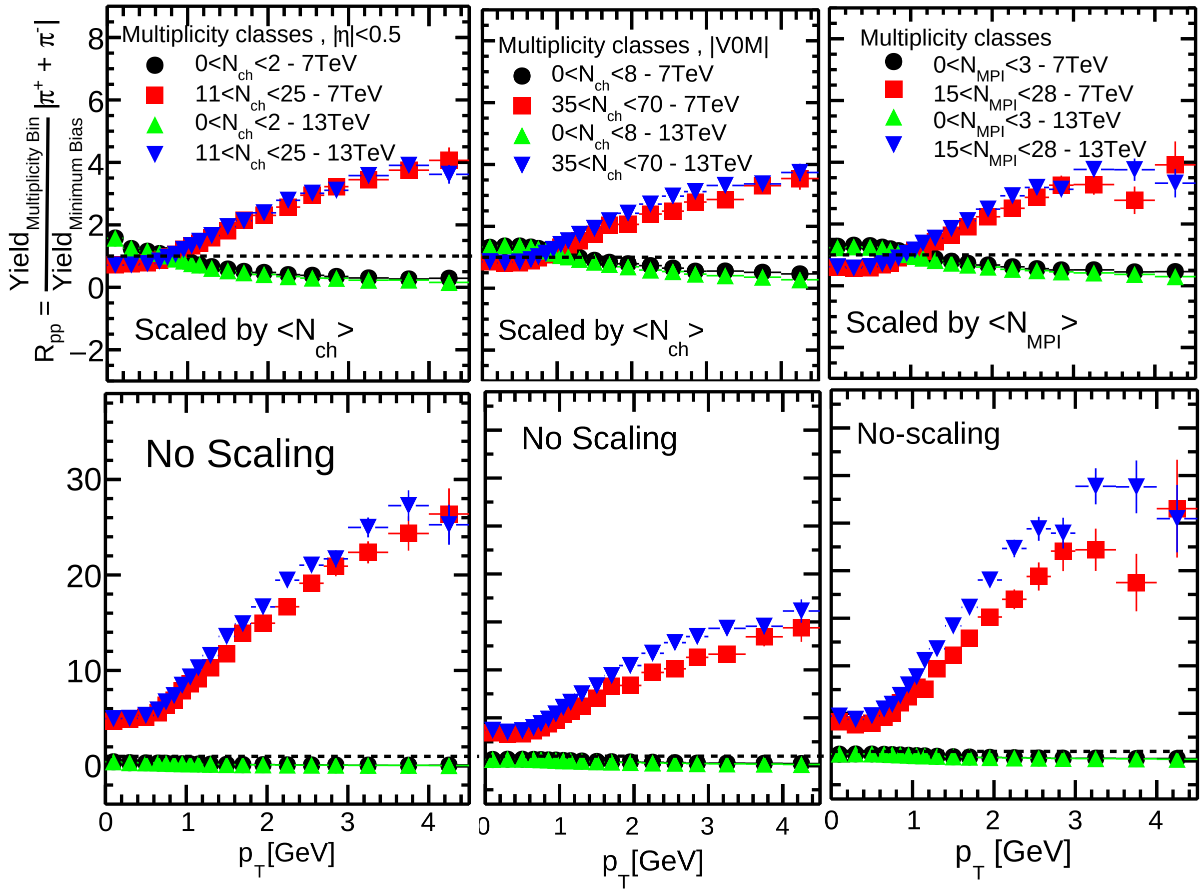

Figure 4.4: (Color online) panel - 1(from left): R_{pp} of pion as a function of charged particle multiplicity in mid rapidity region. panel - 2: R_{pp} of pion as a function of charged particle multiplicity in forward rapidity region. panel - 3: R_{pp} of pion as a function of number of multi-parton interactions for inclusive hard processes using PYTHIA8. The vertical lines in data points are the statistical uncertainties.

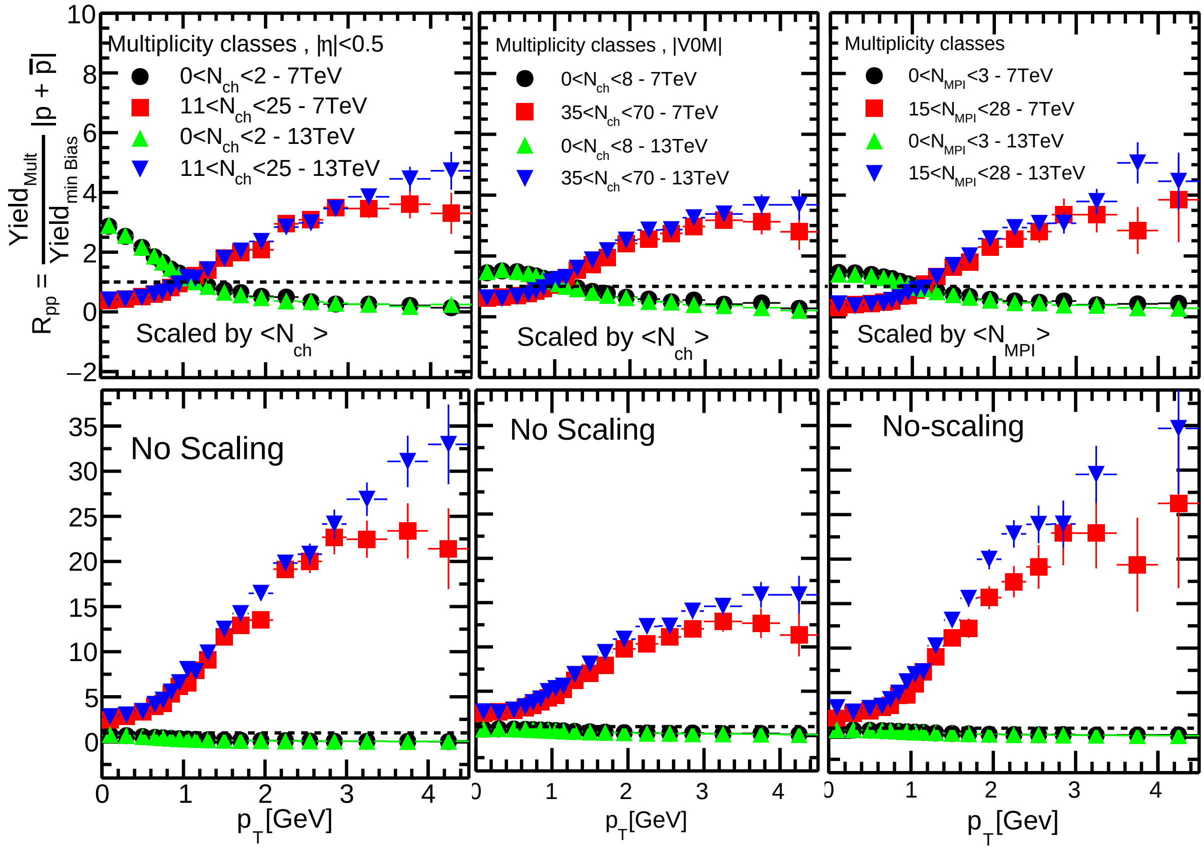

Figure 4.5: (Color online) panel - 1(from left): R_{pp} of proton as a function of charged particle multiplicity in mid rapidity region. panel - 2: R_{pp} of proton as a function of charged particle multiplicity in forward rapidity region. panel - 3: R_{pp} of proton as a function of number of multi-parton interactions for inclusive hard processes using PYTHIA8. The vertical lines in data points are the statistical uncertainties.

4.2 Mean p_T analysis

The normalised mean p_T of proton, kaon and pion for both Color reconnection "ON" and "OFF" as a function of N_{ch} for different rapidity($|\eta| < 0.5$ and V0M) and function of nMPI is plotted (Figures 4.6 4.7 4.8). We observe that for all the three particles under consideration, the normalised mean p_T increases with multiplicity for both N_{ch} and nMPI at both 7 TeV and 13 TeV. Where Deviation from CR - ON is

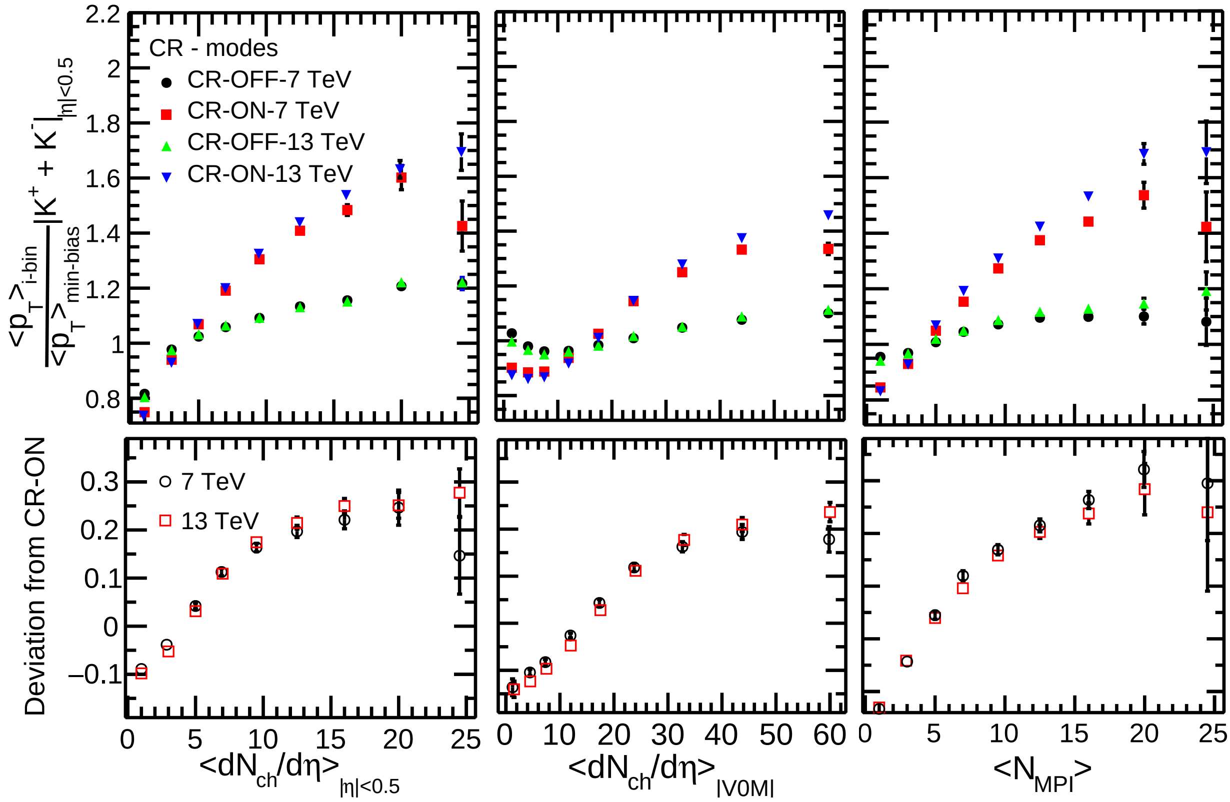

Figure 4.6: (Color online) panel - 1(from left): Normalised mean $< p_T >$ of kaon as a function of charged particle multiplicity in mid rapidity region. panel - 2: Normalised mean $< p_T >$ of kaon as a function of charged particle multiplicity in forward rapidity region. panel - 3: Normalised mean $< p_T >$ of kaon as a function of number of multi-parton interactions for inclusive hard processes using PYTHA8. The vertical lines in data points are the statistical uncertainties.

defined as,

$$Deviation \quad from \quad CR-ON = \frac{Value_{CR-ON} - Value_{CR-OFF}}{Value_{CR-ON}} \tag{4.4}$$

It is observed that the deviation is almost same for both 7 TeV and 13 TeV for all the three scales.

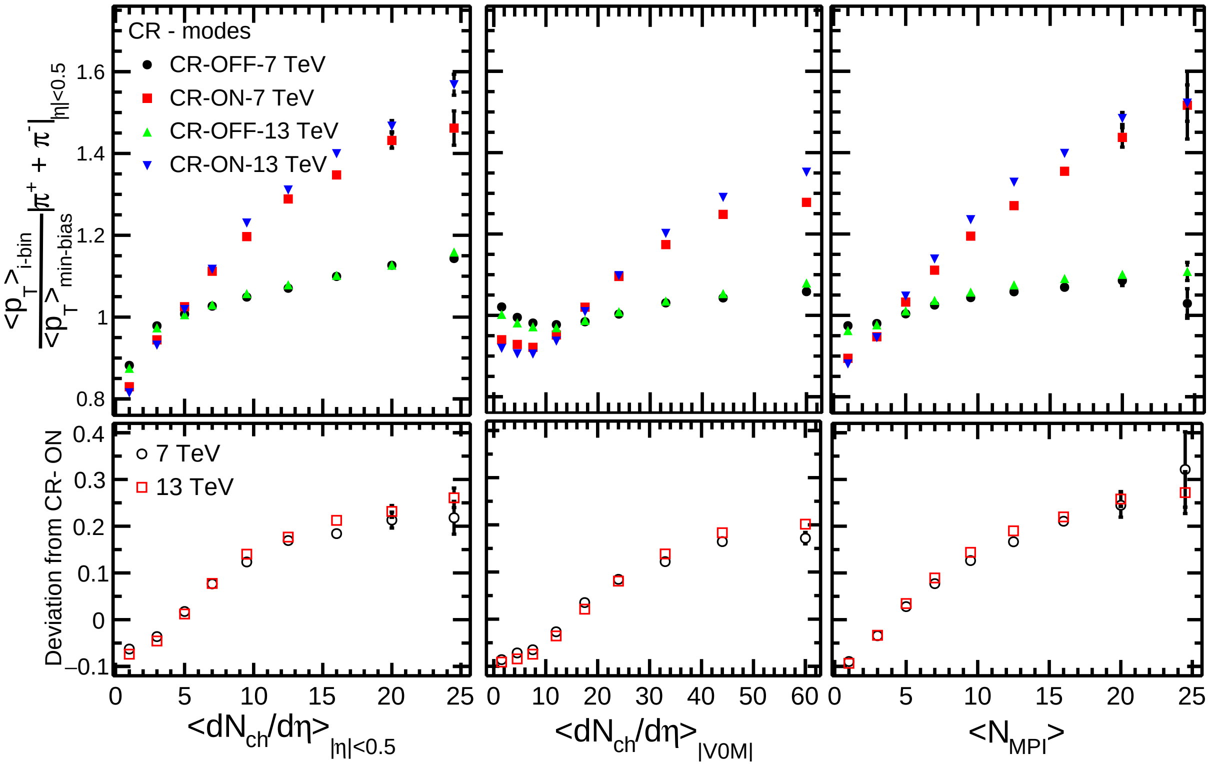

Figure 4.7: (Color online) panel - 1(from left): Normalised mean $< p_T >$ of pion as a function of charged particle multiplicity in mid rapidity region. panel - 2: Normalised mean $< p_T >$ of pion as a function of charged particle multiplicity in forward rapidity region. panel - 3: Normalised mean $< p_T >$ of pion as a function of number of multi-parton interactions for inclusive hard processes using PYTHA8. The vertical lines in data points are the statistical uncertainties.

4.3 Particle production analysis

To understand the production and energy dependence of different particles in proton proton collision, we plotted integrated yield of such particles as function of multiplicity at two different centre-of-mass energies (7 and 13 TeV) for different particles ($\pi^+ + \pi^-, K^+ + K^-, p + \bar{p}$, Λ, ϕ and K^{*0}) (Figures 4.9 4.10 4.11) . It is observed that integrated yield is independent of energy and shows linear trends with increase in multiplicity at mid-rapidity. However, integrated yield seems to have lower slope for multiplicity at forward rapidity and N_{MPI} scale. It is also observed that there is certain dependence of energy for K^{*0} for multiplicity at mid-rapidity and N_{MPI} scale, this dependence found to dominate more at mid-rapidity multiplicity scale.

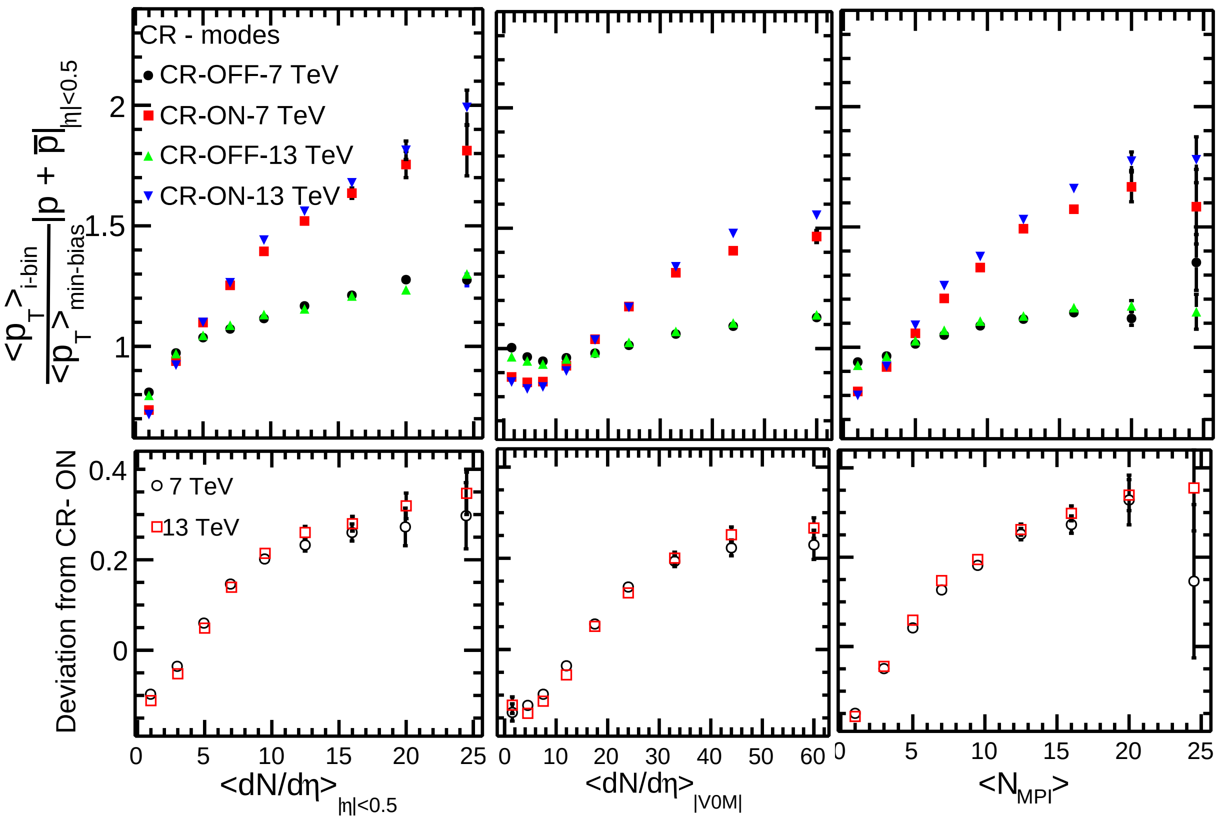

Figure 4.8: (Color online) panel - 1(from left): Normalised mean $< p_T >$ of proton as a function of charged particle multiplicity in mid rapidity region. panel - 2: Normalised mean $< p_T >$ of proton as a function of charged particle multiplicity in forward rapidity region panel - 3: Normalised mean $< p_T >$ of proton as a function of number of multi-parton interactions for inclusive hard processes using PYTHA8. The vertical lines in data points are the statistical uncertainties.

4.4 Particle production ratio analysis

In similar way as previous analysis, ratio of integrated yield of different particle to that of pion $(\pi^+ + \pi^-)$ is calculated and we plotted integrated yield ratio as function of multiplicity at two different centre-of-mass energies (7 and 13 TeV) in three different scales(Figures 4.12 4.13). It is observed that integrated yield ratio of $(K^+ + K^-)/(\pi^+ + \pi^-)$ is higher in all rapidity range and all multipicity compared to $(p + \bar{p})/(\pi^+ + \pi^-)$. This is expected because mass of kaon is lower than proton and according to Boltzmann distribution for given energy production of kaon should be higher than proton. In mid rapidity, proton to pion ratio and kaon to pion ratio is higher in 13 TeV compared to 7 TeV, but this difference is not observed strongly in forward rapidity scale and N_{MPI} scale. Similar conclusions can be given for $\phi/(\pi^+ + \pi^-)$ and $K^{*0}/(\pi^+ + \pi^-)$. The increasing trend in $(K^+ + K^-)/(\pi^+ + \pi^-)$, $\phi/(\pi^+ + \pi^-)$ and $K^{*0}/(\pi^+ + \pi^-)$ ratios hints the possible enhancement of strangeness and decreasing trend in proton to pion ratio hints possible Baryon - Anti baryon anhilation.

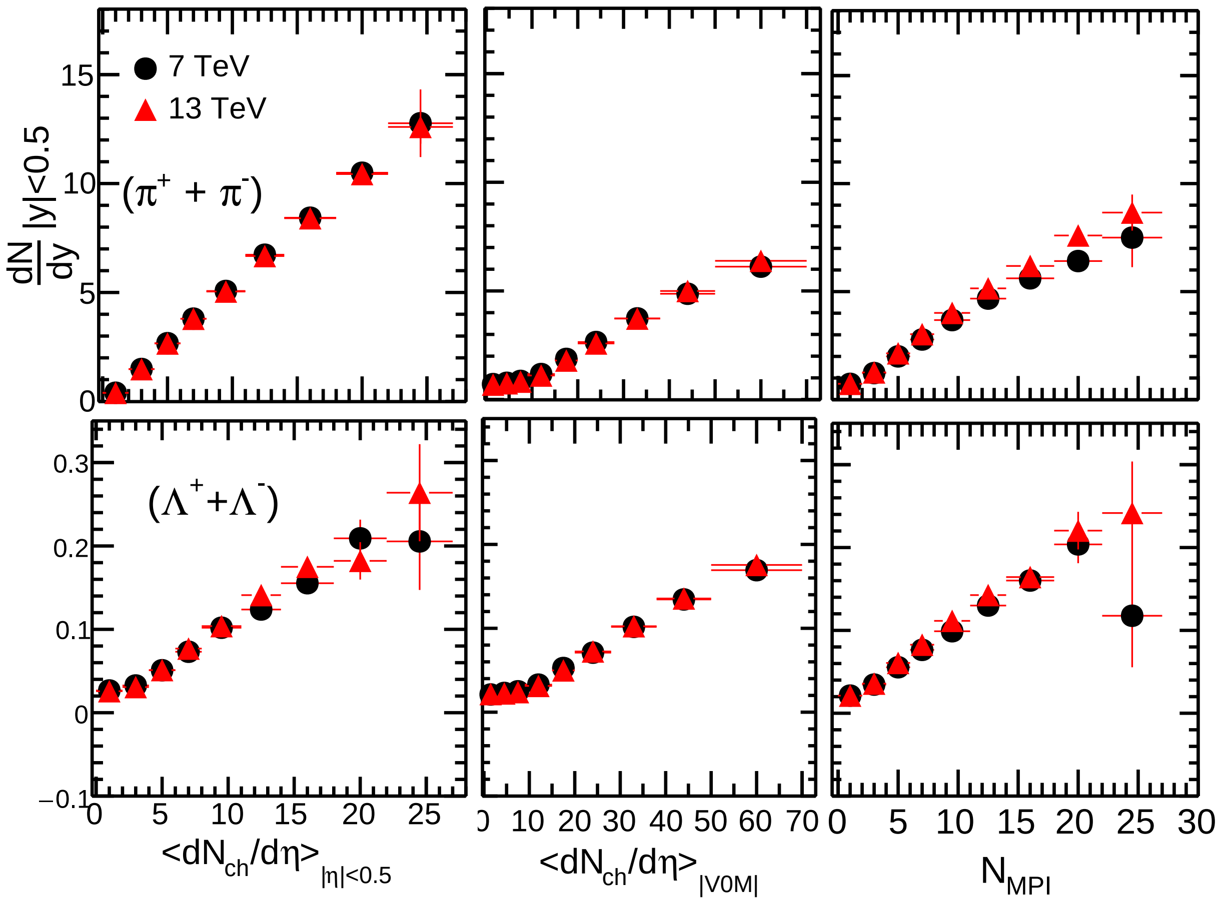

Figure 4.9: (Color online) panel - 1(from left): Particle production of $\Lambda^+ + \Lambda^-$ and $\pi^+ + \pi^-$ as a function of charged particle multiplicity in mid rapidity region. panel - 2: Particle production of $\Lambda^+ + \Lambda^-$ and $\pi^+ + \pi^-$ as a function of charged particle multiplicity in forward rapidity region. panel - 3: Particle production of $\Lambda^+ + \Lambda^-$ and $\pi^+ + \pi^-$ as a function of number of multi-parton interactions for inclusive hard processes using PYTHIA8. The vertical lines in data points are the statistical uncertainties.

4.5 Averaged Particle production

Averaged integrated yield ($\frac{dN}{dy}/ < N_{ch}, \frac{dN}{dy}/ < N_{MPI}$) is plotted at 7 TeV and 13 TeV for $p+\bar{p}$, $K^+ + K^-$, ϕ, K^{*0} at three different scales (Figures 4.14 4.15). Similar trends were observed for ϕ and K^{*0} also energy dependence is found in mid-rapidity scale and N_{MPI} scale. Whereas proton and kaon show no such dependence. Hence the particle production is driven solely by multiplicity.

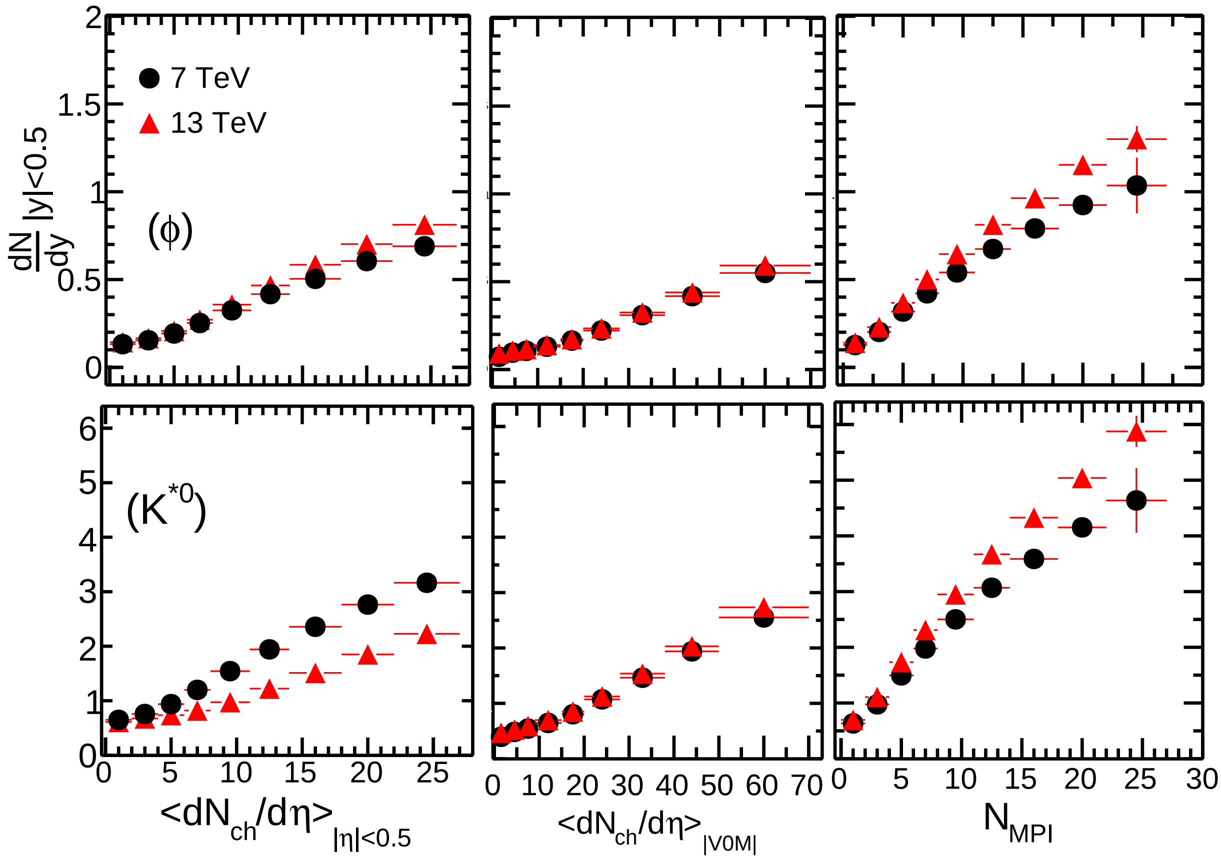

Figure 4.10: (Color online) panel - 1(from left): Particle production of ϕ and K^{*0} as a function of charged particle multiplicity in mid rapidity region. panel - 2: Particle production of ϕ and K^{*0} as a function of charged particle multiplicity in forward rapidity region. panel - 3: Particle production of ϕ and K^{*0} as a function of number of multi-parton interactions for inclusive hard processes using PYTHIA8. The vertical lines in data points are the statistical uncertainties.

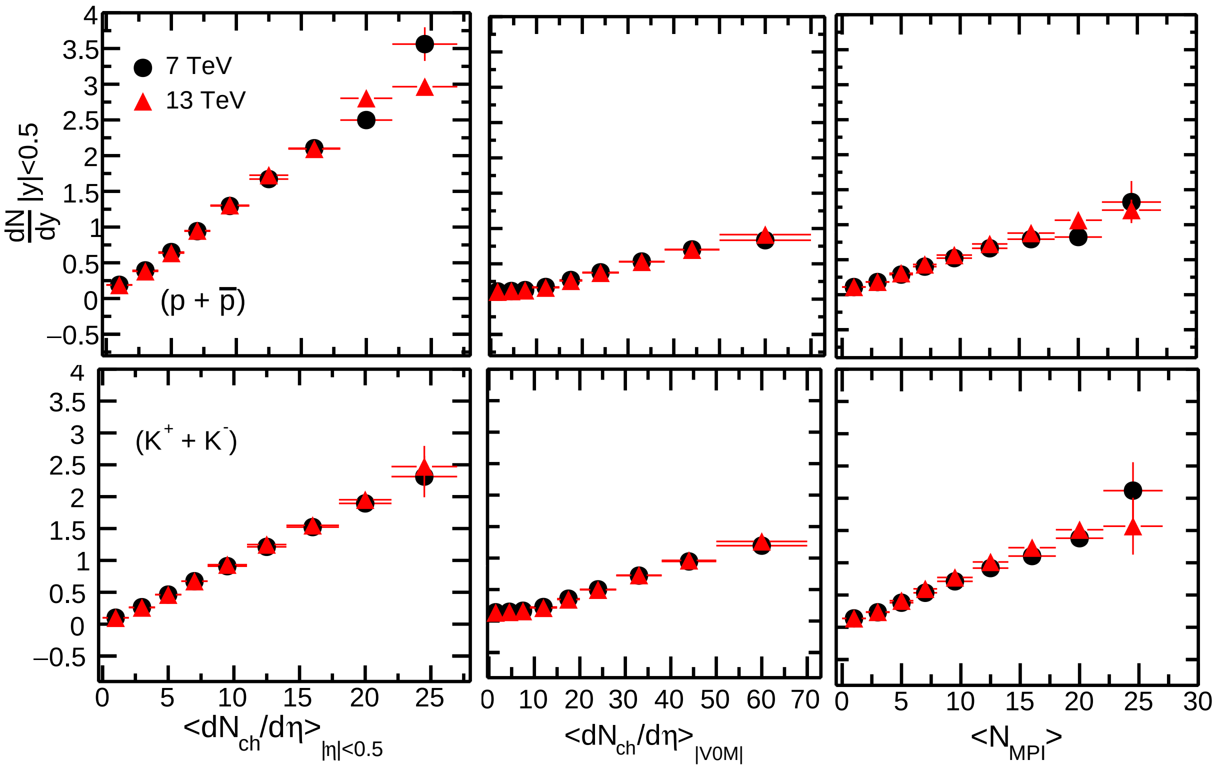

Figure 4.11: (Color online) panel - 1(from left):Particle production of $p + \bar{p}$ and $K^+ + K^-$ as a function of charged particle multiplicity in mid rapidity region. panel - 2: Particle production of $p + \bar{p}$ and $K^+ + K^-$ as a function of charged particle multiplicity in forward rapidity region. panel - 3: Particle production of $p + \bar{p}$ and $K^+ + K^-$ as a function of number of multi-parton interactions for inclusive hard processes using PYTHIA8. The vertical lines in data points are the statistical uncertainties.

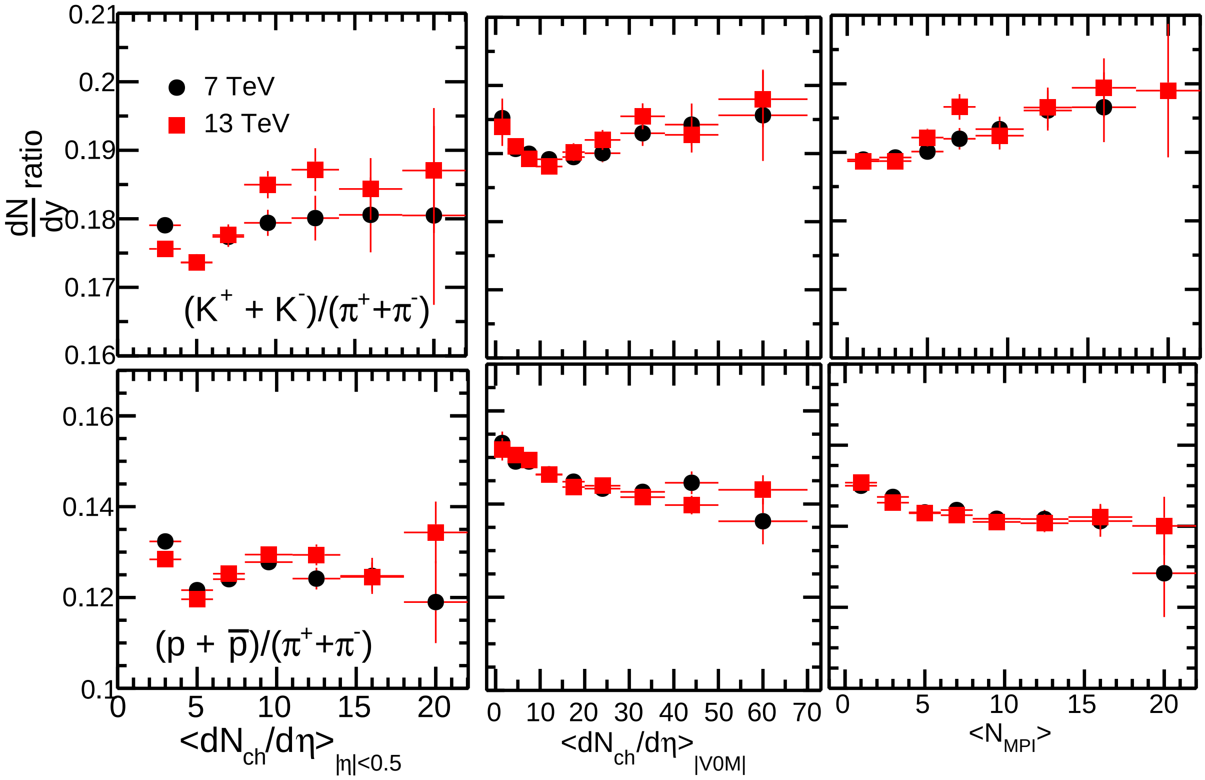

Figure 4.12: (Color online) panel - 1(from left): Particle production ratio of $K^+ + K^-$ and $p + \bar{p}$ to $\pi^+ + \pi^-$ as a function of charged particle multiplicity in mid rapidity region. panel - 2: Particle production ratio of $K^+ + K^-$ and $p + \bar{p}$ to $\pi^+ + \pi^-$ as a function of charged particle multiplicity in forward rapidity region. panel - 3: Particle production ratio of $K^+ + K^-$ and $p + \bar{p}$ to $\pi^+ + \pi^-$ as a function of number of multi-parton interactions for inclusive hard processes using PYTHIA8. The vertical lines in data points are the statistical uncertainties.

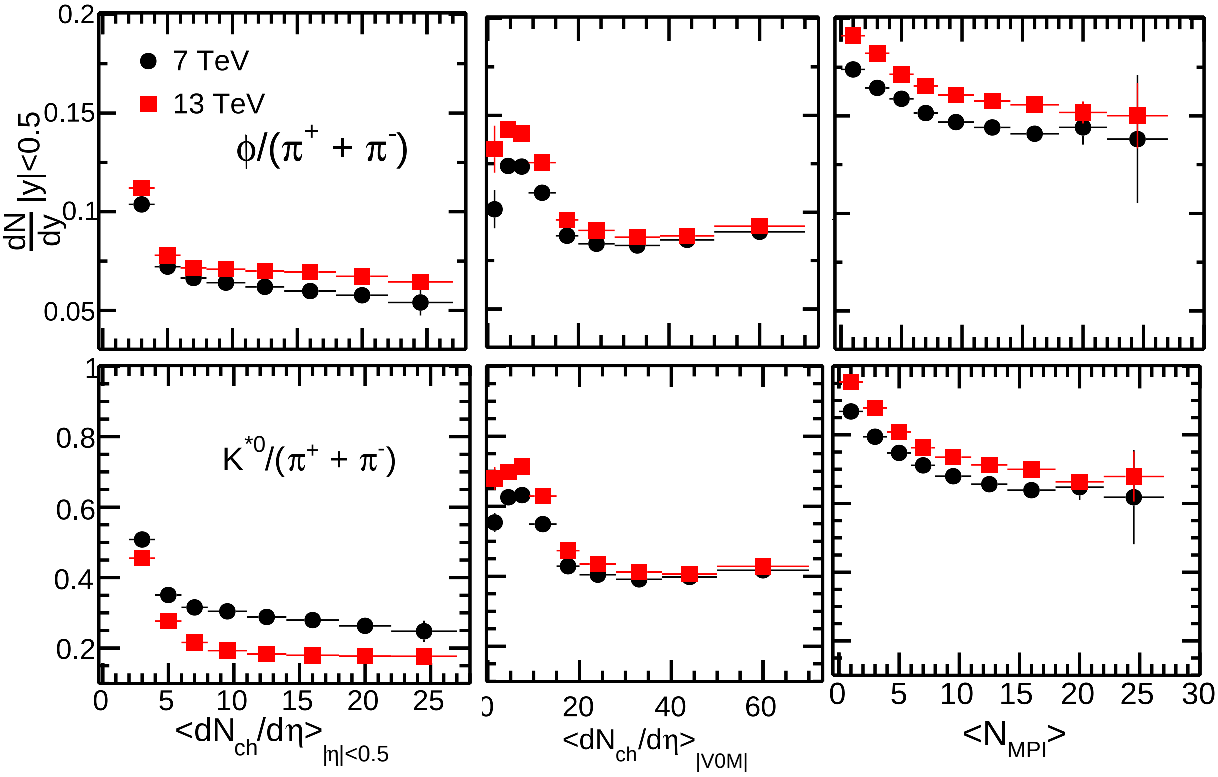

Figure 4.13: (Color online) panel - 1(from left): Particle production ratio of and K^{*0} to $\pi^+ + \pi^-$ as a function of charged particle multiplicity in mid rapidity region. panel - 2: Particle production ratio of and K^{*0} to $\pi^+ + \pi^-$ as a function of charged particle multiplicity in forward rapidity region. panel - 3: Particle production ratio of and K^{*0} to $\pi^+ + \pi^-$ as a function of number of multi-parton interactions for inclusive hard processes using PYTHIA8. The vertical lines in data points are the statistical uncertainties.

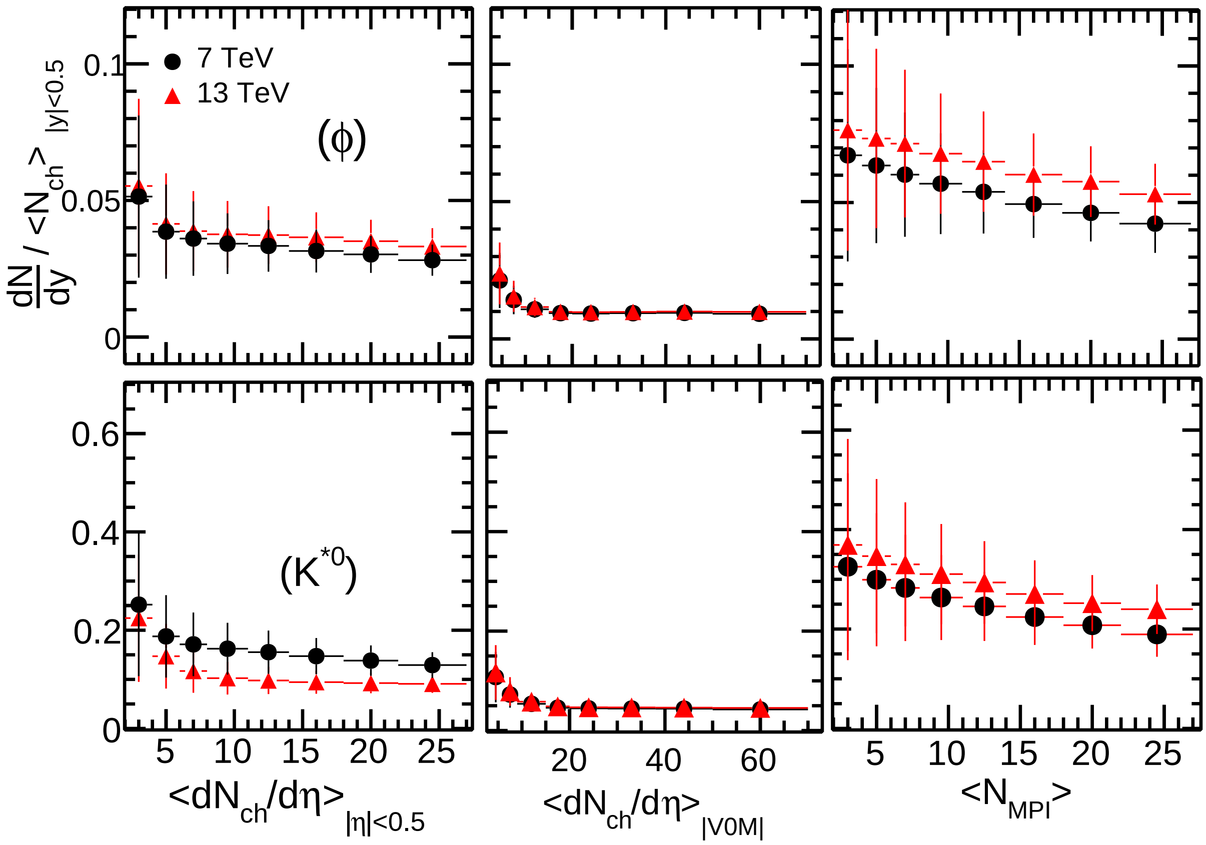

Figure 4.14: (Color online) panel - 1(from left):Averaged Particle production of ϕ and K^{*0} as a function of averaged charged particle multiplicity in mid rapidity region. panel - 2: Averaged Particle production of ϕ and K^{*0} as a function of averaged charged particle multiplicity in forward rapidity region. panel - 3: Averaged Particle production of ϕ and K^{*0} as a function of averaged number of multiparton interactions for inclusive hard processes using PYTHIA8. The vertical lines in data points are the statistical uncertainties.

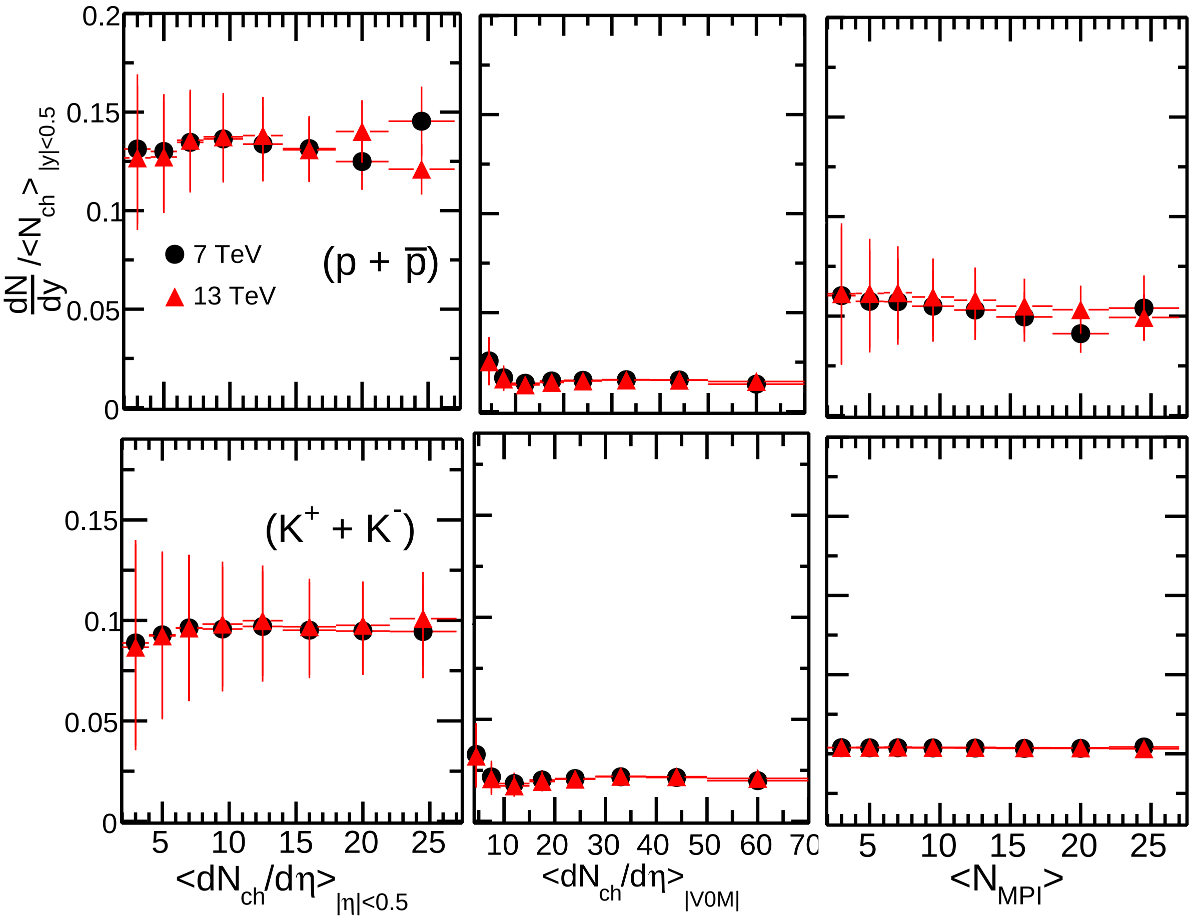

Figure 4.15: (Color online) panel - 1(from left) : Averaged Particle production of $p + \bar{p}$ and $K^{+} + K^{-}$ as a function of charged particle multiplicity in mid rapidity region. panel - 2: Averaged Particle production of $p + \bar{p}$ and $K^{+} + K^{-}$ as a function of Averaged charged particle multiplicity in forward rapidity region. panel - 3: Averaged Particle production of $p + \bar{p}$ and $K^{+} + K^{-}$ as a function of Averaged number of multi-parton interactions for inclusive hard processes using PYTHIA8. The vertical lines in data points are the statistical uncertainties.

Chapter 5

Summary

Calculation methodology for number of binary parton collisions in Glauber framework model for proton proton collisions assuming proton to be composite extended object having three effective quarks and gluon flux tubes within connecting each quarks is explained. Charged particle distribution for proton proton collisions at $\sqrt{s} = 7 TeV$ is obtained using the model under consideration and is compared with ALICE published data.
Using PYTHIA event generator R_{pp} is calculated for proton, pion, kaon at $\sqrt{s} = 7$ TeV and 13 TeV in N_{ch} (both mid rapidity and forward rapidity) and nMPI scale and observed that production mechanism is different for low and high multiplicities. Analysis is extended to calculate mean p_T for same energies and same scale but with and without Color-Reconnection mechanism.

Integrated yield for the identified particles are calculated as function of nMPI at $\sqrt{s} = 7$ TeV and 13 TeV and similar trend is obtained for mid-rapidity N_{ch} scale and nMPI scale. Interesting to note that production mechanism is same for both $\sqrt{s} = 7$ TeV and 13 TeV. Also ratio of integrated yields of $p^{\pm}$, $K^{\pm}$, ϕ and K^{*0} to that of $\pi^{\pm}$ is found for nMPI scale. Multiplicity dependence of Averaged yield of identified particles is calculated and found that the production is driven by multiplicity.

Possible extension of N_{coll} calculations can be done by calculating R_{pp} by separating different multiplicity bins for the N_{ch} distribution obtained. And analysis can be repeated for different energies to fine tune parameters used in the model.

Chapter 6

Appendix

6.1 Appendix A

Here Rotation matrix given in section 2.1 is discussed. According to Euler rotation theorem any rotation can be given using three angles (γ, β, α). Hence overall rotation is given by,

$$\mathscr{R}(\alpha, \beta, \gamma) = \mathscr{R}_Z(\gamma)\mathscr{R}_Y(\beta)\mathscr{R}_Z(\alpha) \tag{6.1}$$

Where $\mathscr{R}_Z(\gamma)$ represent rotation about Z-axis by an angle γ similarly $\mathscr{R}_Z(\alpha)$ by angle α and $\mathscr{R}_Y(\beta)$ represent rotation about Y-axis by an angle β (all 3×3 matrices).

Given initial position vector $\mathbf{a} = (0, 0, 1)$ and the final rotated vector
$\mathbf{b} = (cos\phi sin\theta, sin\phi cos\theta, cos\theta)$, hence relating these vectors (considering vectors to be column matrix)

$$\mathbf{b} = \mathscr{R}(\alpha, \beta, \gamma)\mathbf{a} \tag{6.2}$$

After substituting matrices and relating euler angles with spherical angles we get, $\beta = \theta$, $\alpha = 0$, $\gamma = -\phi$. Hence the explicit form of the rotation matrix is given by

$$\mathscr{R}(\theta, \phi) = \begin{bmatrix} \cos\theta\cos\phi & -\sin\phi & \cos\phi\sin\theta \\ \sin\phi\cos\theta & \cos\phi & \sin\phi\sin\theta \\ -\sin\theta & 0 & \cos\theta \end{bmatrix} \tag{6.3}$$

6.2 Appendix B

Definitions for the variables used in this work assuming incident beam is in the z-direction.

1. Rapidity

$$y = \frac{1}{2} ln\left(\frac{1+\beta}{1-\beta}\right) \tag{6.4}$$

On successive Lorentz boost the velocity is not a additive quantity, hence rapidity is defined as in the equation 6.4 which is an additive quantity. In experiments alternative way of defining rapidity is,

$$y = \frac{1}{2} ln\left(\frac{E+p_z}{E-p_z}\right) \tag{6.5}$$

2. Pseudo - Rapidity

At high energies all particles have $E \approx pc$ hence the rapidity in equation 6.5 is approximated called Pseudo - Rapidity and defined as,

$$\eta = -ln \tan(\frac{\theta}{2}) \tag{6.6}$$

3. Transverse momentum

The momentum 3 vector components can be decomposed into the longitudinal (p_z) and the transverse (p_T), p_T being a vector quantity which is invariant under a Lorentz boost along the longitudinal direction. And it is defined as,

$$p_T = \sqrt{p_x^2 + p_y^2} \tag{6.7}$$

Bibliography

[1] L. B. Okun, “Leptons and Quarks : Special Edition Commemorating the Discovery of the Higgs Boson,”

[2] K. I. Kondo, “Abelian projected effective gauge theory of QCD with asymptotic freedom and quark confinement,” Prog. Theor. Phys. Suppl. **131**, 243 (1998)

[3] G. V. Efimov and M. A. Ivanov, “The Quark confinement model of hadrons,”

[4] L. Susskind, “Lattice Models of Quark Confinement at High Temperature,” Phys. Rev. D **20**, 2610 (1979).

[5] C. Klein-Bösing [ALICE Collaboration], “New Results on Hard Probes in Heavy-Ion Collisions with ALICE,” PoS LHCP **2018**, 222 (2018)

[6] T. Sjostrand and M. van Zijl, “A Multiple Interaction Model for the Event Structure in Hadron Collisions,” Phys. Rev. D **36**, 2019 (1987).

[7] B. Andersson, G. Gustafson, G. Ingelman and T. Sjostrand, “Parton Fragmentation and String Dynamics,” Phys. Rept. **97**, 31 (1983).

[8] T. Sjöstrand *et al.*, “An Introduction to PYTHIA 8.2,” Comput. Phys. Commun. **191**, 159 (2015) łazek2012łazek2012

[9] S. D. Glazek, “Hypothesis of Quark Binding by Condensation of Gluons in Hadrons,” Few Body Syst. **52**, 367 (2012)

[10] P. Bartalini *et al.*, “Multi-Parton Interactions at the LHC,” arXiv:1111.0469 [hep-ph].

[11] E. Di Salvo, “Removing The Low P(t) Divergence In Hard Hadron Hadron Collisions At High-energies,” Nuovo Cim. A **99**, 135 (1988).

[12] E. Cuautle, A. Ortiz and G. Paic, “Effects produced by multi-parton interactions and color reconnection in small systems,” Nucl. Phys. A **956**, 749 (2016).

[13] E. L. Bratkovskaya, O. Linnyk, V. P. Konchakovski, M. I. Gorenstein and W. Cassing, “Signatures of the strongly interacting QGP in relativistic heavy-ion collisions,”.

[14] M. T. AlFiky, O. T. ElSherif and A. M. Hamed, “Quark Gluon Plasma Formation in proton proton Collisions Using PYTHIA,”.

[15] C. Loizides, J. Kamin and D. d'Enterria, "Improved Monte Carlo Glauber predictions at present and future nuclear colliders," Phys. Rev. C **97**, no. 5, 054910 (2018).

[16] K. J. Gonçalves, A. V. Giannini, D. D. Chinellato and G. Torrieri, "Limiting fragmentation as an initial state probe in heavy ion collisions,"

[17] W. Busza, K. Rajagopal and W. van der Schee, Ann. Rev. Nucl. Part. Sci. **68**, 339 (2018) doi:10.1146/annurev-nucl-101917-020852 [arXiv:1802.04801 [hep-ph]].

[18] U. Heinz and R. Snellings, Ann. Rev. Nucl. Part. Sci. **63**, 123 (2013) doi:10.1146/annurev-nucl-102212-170540 [arXiv:1301.2826 [nucl-th]].

[19] J. Adam *et al.* [ALICE Collaboration], 'Enhanced production of multi-strange hadrons in high-multiplicity proton proton collisions," Nature Phys. **13**, 535 (2017) doi:10.1038/nphys4111 [arXiv:1606.07424 [nucl-ex]].